Can vertical migrations of dinoflagellates explain observed bioluminescence patterns during an upwelling event in Monterey Bay, California?

Igor Shulman, Bradley Penta, Mark A. Moline, Steven H. D. Haddock, Stephanie Anderson, Matthew J. Oliver, and Peter Sakalaukus

[1] Extensive AUVs surveys showed that during the development of upwelling, bioluminescent dinoflagellates from the northern part of the Monterey Bay, California (called the upwelling shadow area), were able to avoid advection by southward flowing currents along the entrance to the Bay, while non-bioluminescent phytoplankton were advected by currents. It is known that vertical swimming of dinoflagellates to deeper layers helps them avoid losses due to advection. In the present paper, we investigate if modeling dinoflagellates' vertical swimming can explain the observed dinoflagellates' ability to avoid advection during the upwelling development. The dynamics of a dinoflagellate population is modeled with the tracer model with introduced vertical swimming velocity. Three swimming behaviors are considered: sinking, swimming to the target depth and diel vertical migration. Velocities in all swimming cases are considered in the ranges of documented velocities for the observed dinoflagellates species during the upwelling development in the Monterey Bay. Our modeling confirmed that observed bioluminescent dinoflagellates' avoidance of advection during the upwelling development can be explained by their vertical swimming ability. In the case of swimming with 20 m/day (which is half of observed maximum swimming velocity), around 40% of dinoflagellates population from the northern part of the Bay were advected along the entrance to the Bay in comparison to the case without swimming. This is in agreement with the ratio of around 45% of observed mean bioluminescence intensity at the entrance to the Bay to the observed mean intensity in the northern part of the Bay. This mechanism also helps explain the general persistence of dinoflagellates in this part of the coastline.

1. Introduction

[2] The northern part of the Monterey Bay, California, is known as a biologically active area, and so-called upwelling shadow area, where dense phytoplankton blooms have been observed [*Graham and Largier*, 1997; *Ryan et al.*, 2005, 2008]. In our previous study, observations of physical, bio-optical properties (including bioluminescence) together with results from dynamical biochemical and bioluminescence models were used to interpret the development of the August 2003 upwelling in Monterey Bay, California [*Shulman et al.*, 2011]. Our analysis showed that during the upwelling, bioluminescent dinoflagellates from the northern part of the Bay were able to avoid advection by strong southward currents developed during the upwelling event. Non-bioluminescent phytoplankton were advected. Results from the dynamical bioluminescence model showed high values of bioluminescence intensity (BL) along the entrance to the Bay [*Shulman et al.*, 2011], which was not in agreement with the observed BL. In the model, the BL dynamics were controlled by advective and diffusive processes only, and as it was speculated by *Shulman et al.* [2011], the lack of modeling of behavioral dynamics of bioluminescent organisms, as well as modeling of growth and loss terms, are responsible for the BL model's inability to predict the observed weakening of the BL intensity along the entrance to the Bay.

[3] Why were bioluminescent dinoflagellates not advected by the southward flow? Previous studies [*Smayda*,

2010b; *Kudela et al.*, 2010] suggest that dinoflagellates exhibit environmentally induced adaptation and survival to changing environmental conditions. As stated by *Smayda* [2010b, pp. 82–83], "…vertical migration is a fundamental trait in which directional swimming helps dinoflagellates to optimize growth and survival…Avoidance migrations to deeper layers can reduce advective loss, allow local retention of species and prolong their blooms." The observed seasonal persistence of dinoflagellates [*Ryan et al.*, 2005, 2009] might be a result of vertical migration of the dinoflagellates to retain their population in the northern part of Monterey Bay.

[4] The objective of the present paper is to address the following question: whether modeling of bioluminescent dinoflagellates' vertical swimming behavior can explain the observed dinoflagellates' avoidance to be advected by strong currents during the August 2003 upwelling event. The dinoflagellates swimming behavior depends on many factors including: concentration of their population, physical conditions (currents, temperature, strength of stratification, mixed layer depth etc.), light limitation and inhibition, nutrients availability, prey pressure, etc. [see, e.g., *Smayda*, 2000; *Kamykowski et al.*, 1988]. In this case, the simulation of actual dinoflagellates swimming during the 2003 upwelling event represents a very challenging task and requires knowledge of their initial concentration and accurate modeling as physical, as well as biological-optical environmental conditions during the event. For this reason, in the present paper we deploy a simpler approach (details of which are described in section 3) to address the objective of the paper. The dynamics of dinoflagellates is modeled with the tracer model where the dinoflagellate population is modeled as a concentration, and vertical swimming velocity is introduced into the tracer advective-diffusive-reaction model. Three swimming behaviors are considered here: sinking, swimming to the target depth, and diel vertical migration [*Franks*, 1992]. Swimming velocities in all cases are considered in the range of documented velocities for the dinoflagellates species observed during the upwelling in the Monterey Bay. We compare the advected fraction of the tracer concentration in the case of no swimming to the advected fractions of tracer concentrations in cases of the discussed above swimming strategies. The main challenge with the forward integration of the tracer model is the high level of uncertainty in the initial distribution of dinoflagellates concentration in the northern part of the bay. However, the knowledge of the initial distribution of the dinoflagellates in the northern part of the Bay is not needed if we use an adjoint to the tracer model. The distribution of the adjoint to the tracer model represents the fraction of tracer concentration which will be circulated from the northern part of the Bay along the entrance to the Bay. For this reason, numerical experiments with the integration of the adjoint to the tracer model, as well as experiments of forward integration of the tracer model, are used in the present study.

[5] The structure of the paper is the following: the upwelling event of August 2003 is described in section 2. Section 3 is devoted to methods and includes descriptions of a biochemical, physical model, the BL model, the tracer model (with swimming behavior modeling), and its adjoint. Modeling results are presented in section 4, and section 5 is devoted to conclusions.

2. Description of Bio-optical and Physical Properties During the Upwelling Event

[6] In this section we briefly repeat the description of the August 2003 upwelling event presented in section 3 of *Shulman et al.* [2011]. Figure 1 shows HF radar surface currents and the subsurface profiles of northward and eastward velocity components at mooring M1. Both surface and subsurface currents are averaged over three days of upwelling (15–17 August). The circulation patterns show the development of a strong, wide southward flow along the entrance to the Bay, which extends up to 150 m in depth. This southward flow separates a pair of cyclonic (inside the Bay) and anticyclonic circulations. As we mentioned in section 1, the northern part of the bay (so-called upwelling shadow area (SA) (Figure 1)) is known as a biologically active area, and where dense phytoplankton blooms have been observed [*Graham and Largier*, 1997; *Ryan et al.*, 2005, 2008]. Figure 2 shows chlorophyll, bioluminescence (BL) and backscatter surveys [*Moline et al.*, 2009; *Shulman et al.*, 2011] conducted by REMUS autonomous underwater vehicle (AUV) along a V-shaped transect (Figure 1). The REMUS transect began near Santa Cruz in the SA, ran out to the buoy M1 (Figure 1), and then returned back to shore. Inshore AUV observations (in the SA area) show the consistent coincidence of chlorophyll, backscatter, and BL maxima during upwelling development. Offshore AUV observations (taken at the entrance to the Bay) show deeper BL maxima below the surface layers of high chlorophyll and backscatter values during the earlier stage of the upwelling development. The inshore BL maxima are associated with phytoplankton (dinoflagellates), while offshore BL maxima are due to larger zooplankton, which is in agreement with general differences in flash kinetics between planktonic dinoflagellates and zooplankton presented by *Moline et al.* [2009]. The observed deep offshore BL maximum disappeared during the upwelling development and became a shallower and much weaker signal coinciding with high chlorophyll and backscatter values offshore. Observations together with modeling results [*Shulman et al.*, 2011] suggest that, with the development of upwelling, the offshore water masses (with the subsurface layer of bioluminescent zooplankton) were advected southward and replaced with water masses showing relatively high values of chlorophyll fluorescence and backscatter. This high presence of phytoplankton at the entrance to the Bay is a result of its advection from the northern coast of the Bay (SA area) by the strong southward flow (Figure 1). Because there is a weak observed BL signal around mooring M1 (Figure 2), mostly non-bioluminescent phytoplankton were advected from the north. The bioluminescent dinoflagellates species were able to avoid the strong advection along the entrance to the Bay.

3. Methods

3.1. The Biochemical, Physical Model of the Monterey Bay

[7] The Monterey Bay model (called the NCOM ICON) consists of the physical model [*Shulman et al.*, 2011], which

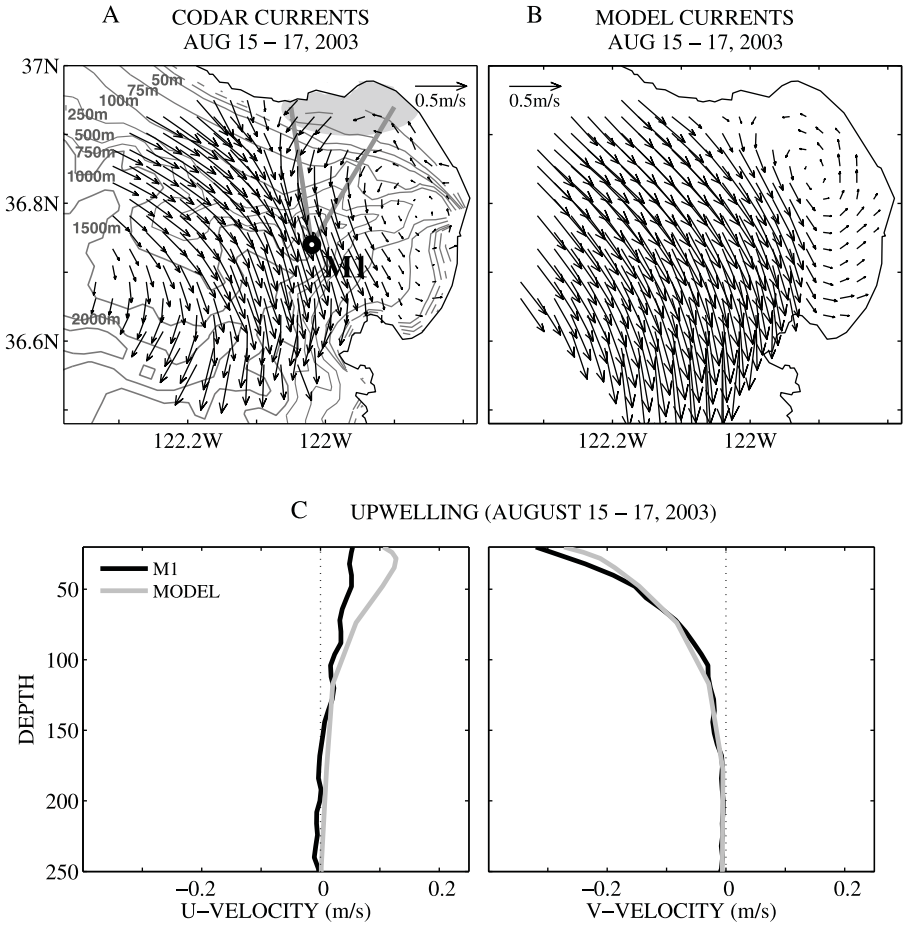

Figure 1. (a) HF radar surface currents averaged over three days of upwelling (15–17 August 2003). Location of mooring M1, V-shaped transect of CalPoly AUV REMUS, location of the shadow upwelling area (SA, shaded area in the northern part of the Bay), and bathymetric contours are also shown. (b) Model-predicted surface currents averaged over three days of upwelling (15–17 August 2003). Model currents are plotted at locations of HF radar footprints. (c) ADCP observed (black lines) and model-predicted (shaded lines) subsurface profiles of the velocity components at the M1 mooring. Observed and model-predicted profiles are averaged over three days of upwelling. U is the eastward and V is the northward component of velocity.

is coupled to the biochemical model [*Chai et al.*, 2002]. The physical model of the Monterey Bay is based on the NCOM model, which is a primitive-equation, 3D, hydrostatic model. It uses the Mellor-Yamada level 2.5 turbulence closure scheme, and the Smagorinsky formulation for horizontal mixing [*Martin*, 2000].

[8] The NCOM ICON model is set up on a curvilinear orthogonal grid with resolution ranging from 1 to 4 km. The model is forced with surface fluxes from the Coupled Ocean and Atmospheric Mesoscale Prediction System (COAMPS) [*Doyle et al.*, 2009] at 3 km horizontal resolution. The 3-km resolution COAMPS grid mesh is centered over Central California and the Monterey Bay. Phytoplankton photosynthesis in the biochemical model is driven by Photosynthetically Active Radiation (PAR), which is estimated based on the shortwave radiation flux from the COAMPS model. The *Penta et al.* [2008] scheme is used for PAR attenuation with depth.

[9] The NCOM ICON model uses the Navy Coupled Ocean Data Assimilation (NCODA) system [*Cummings*, 2005] for the assimilation of the temperature and salinity data from different observational platforms. The NCODA is a fully 3D multivariate optimum interpolation system. Assimilation of temperature and salinity data is performed every 12 h (assimilation cycle). Differences between the NCODA analysis and the model forecast are uniformly added to the model temperature and salinity fields over the assimilation cycle [*Shulman et al.*, 2010]. Open boundary conditions for the NCOM ICON are derived from the regional model of the California Current (NCOM CCS) [*Shulman et al.*, 2007]. The NCOM CCS has a horizontal resolution of about 9 km and, the model is forced with atmospheric products derived from the COAMPS [*Doyle et al.*, 2009].

[10] Open boundary conditions for the regional NCOM CCS model are derived from the NCOM global model [*Rhodes et al.*, 2002; *Barron et al.*, 2004], which has 1/8° horizontal resolution. The model assimilates satellite-derived sea surface height (SSH) and sea surface temperature (SST) data via synthetic temperature and salinity

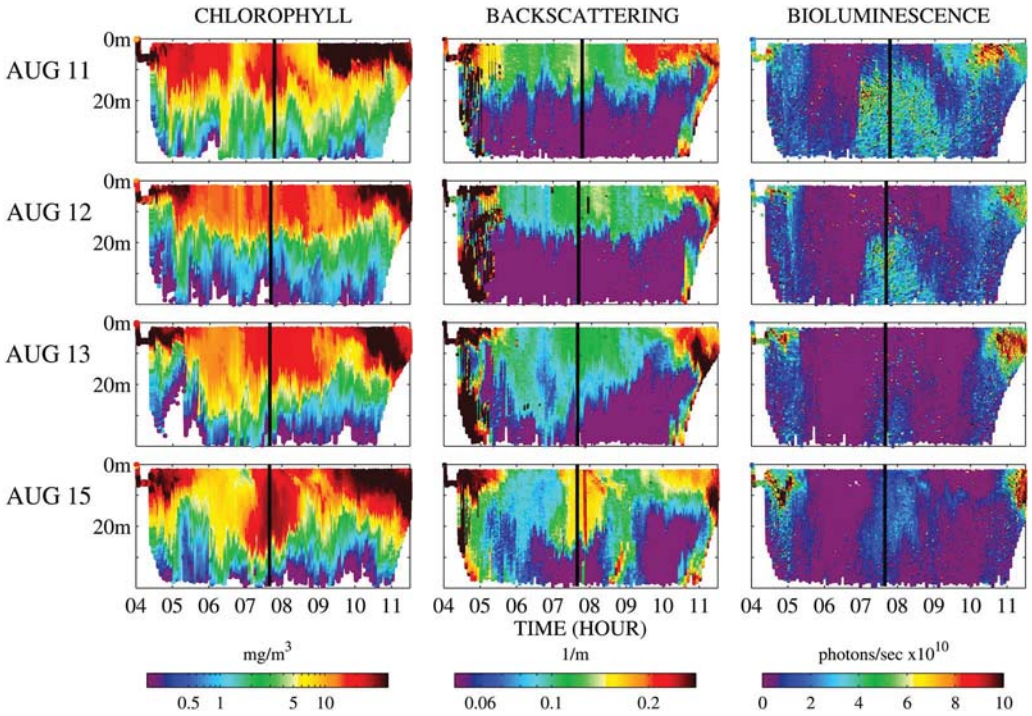

Figure 2. AUV REMUS observed chlorophyll, backscattering and bioluminescence during 11–15 August. Solid vertical lines indicate location of the M1 mooring.

profiles derived from the Modular Ocean Data Assimilation System (MODAS) [*Fox et al.*, 2002], and uses atmospheric forcing from the Navy Global Atmospheric Prediction System (NOGAPS) [*Rosmond et al.*, 2002].

[11] Comparisons of COAMPS August 2003 predictions with aircraft and mooring observations were reported by *Ramp et al.* [2009], *Doyle et al.* [2009], *Shulman et al.* [2009] and *Shulman et al.* [2010]. Good spatial agreement between aircraft and COAMPS winds for 15 August 2003 was demonstrated in Figure 3 of *Ramp et al.* [2009]. Both, aircraft observed and COAMPS winds showed the weakening of winds in the upwelling shadow area.

[12] The NCOM ICON physical model predictions during the upwelling event of August 2003 were evaluated in previous studies [*Shulman et al.*, 2009, 2010]. Figure 1 shows comparison of HF radar surface currents and model-predicted surface currents, as well as comparisons of subsurface profiles of northward and eastward velocity components at mooring M1. There is a good agreement between observed and model-predicted currents, especially in predictions of southward component of the velocity at the mooring M1 location (Figure 1c).

3.2. The Bioluminescence Model

[13] The bioluminescence model (BL model) is based on BL predictions with an advection–diffusion-reaction model (ADR) [*Shulman et al.*, 2005]:

$$\frac{\partial C}{\partial t} = -\frac{\partial}{\partial x}(Cu) - \frac{\partial}{\partial y}(Cv) - \frac{\partial}{\partial z}(Cw) + \nabla\cdot(A\nabla C) + S(x,y,z,t), \quad (1)$$

where BL is modeled as concentration $C(x, y, z, t)$, $A(x, y, z, t)$ are horizontal and vertical diffusivities, (u, v, w) are components of fluid velocity taken from the NCOM ICON model, and $S(x, y, z, t)$ is the source minus sink term for C.

[14] For initialization on 14 August 00Z, available BL observations (data from four AUVs sections [*Shulman et al.*, 2011]) are assimilated into the above ADR model by using the source term S(x, y, z, t) in the following form [*Shulman et al.*, 2005]:

$$S(x,y,z,t) = \gamma(C - C^0)\delta(\tau - \tau^0), \quad (2)$$

where C^0 are BL observations, γ is the scalar nudging coefficient multiplying $(C - C^0)$, τ is the location in the model domain with coordinates (x, y, z), τ^0 is the location of the observed BL (C^0) with coordinates (x^0, y^0, z^0), and $\delta(\tau - \tau^0)$ is a Dirac function for which $\delta = 1$ when $\tau = \tau^0$ and $\delta = 0$ for all other cases.

[15] Velocities and diffusivities in (1) are taken from the initialization day (14 August 2003) and kept unchanged during the initialization-assimilation procedure. In this case, the assimilated BL (concentration C) is spread throughout the model domain until the equilibrium is reached (when the value of $\partial C/\partial t$ is zero in equation (1)). This provides the initial BL distribution, which is dynamically balanced with the physical conditions at the time of the initialization [see *Shulman et al.*, 2005]. The value of γ equal 1/3600 s^{-1} was used. As shown by *Hines and Killworth* [2001], the long-term performance of data assimilation is relatively insensitive to the value of γ, and that smaller values of γ give a slower convergence to the steady state solution.

Table 1. Observed and Modeled Mean BL in Shadow Area (SA) and at M1 ($\times 10^{10}$ photon/sec)

	Observed			Modeled		
	SA	M1	M1/SA (%)	SA	M1	M1/SA
15 Aug.	3.07	1.39	45	2.7	2.4	89
16 Aug.	3.37	0.62	18	2.8	3.5	125
17 Aug.	4.23	0.35	8	3.97	2.56	65

[16] The equilibrium field C is used as the initial tracer distribution for the following prognostic (forward) calculations with the ADR model. During prognostic calculations, the hydrodynamic velocities and diffusivities change in accord with the hydrodynamic model.

[17] As noted by *Shulman et al.* [2011], the initial BL distribution on 14 August as well as the BL distribution after 24 h of forward simulations (on 15 August) demonstrated a strong BL signal in the area around mooring M1, while, as discussed in section 1 (see Figures 1 and 2), a weak BL signal is observed in the M1 area. This is quantified also in Table 1, where observed and model predicted means of BL in the upwelling shadow area (SA) and around M1 mooring are presented. Observations show that the mean BL signal at M1 is more than two times weaker than the mean BL signal in SA on 15 August, and 5 and 12 times weaker on 16 and 17 August respectively. However, the model predicted that mean BL signals are comparable at M1 and SA areas during this period (Table 1). The high values of the concentration C (BL) at M1 are the result of advection by the southward flow of BL concentration from the SA area along the entrance to the Bay. In reality, this advection of bioluminescent phytoplankton did not occur.

3.3. The Tracer Model With the Swimming Behavior and Its Adjoint

[18] In the present study, the evolution of the concentration of bioluminescent dinoflagellates is studied by the following tracer model:

$$\frac{\partial C}{\partial t} = -\frac{\partial}{\partial x}(Cu) - \frac{\partial}{\partial y}(Cv) - \frac{\partial}{\partial z}(C(w+w_s)) + \nabla\cdot(A\nabla C) + \mu C \tag{3}$$

where $C(x, y, z, t)$ is concentration of dinoflagellates, and $A(x, y, z, t)$ are horizontal and vertical diffusivities, (u,v,w) are components of fluid velocity, w_s is dinoflagellates swimming velocity, and μ is the compound rate of growth minus mortality, which we call decay rate because only zero or negative values of μ are considered here. Diffusivities and fluid velocity are from the NCOM ICON model described in section 3.1.

[19] A similar model to (3) was used, for example, by *Stock et al.* [2005] for modeling *Alexandrium fundyense* dinoflagellates bloom in the Gulf of Maine.

[20] The following types of swimming behavior are described by *Franks* [1992]:

[21] a) Sinking or swimming downward

$$w_s(x, y, z, t) = -w_o \tag{4}$$

where w_o is the sinking or swimming downward velocity.

[22] b) Depth-directed swimming

$$w_s(x, y, z) = w_o \tanh\left(\frac{z - z_o}{z_w}\right) \tag{5}$$

where z_0 is a target swimming depth, when organisms swimming downward from the surface, and upward from the depth. The depth z_0 might be the thermocline or nutricline depth, or depth below euphotic zone etc. The scale z_w represents a distance where dinoflagellates slow down approaching the target depth.

[23] c) Floating

[24] Floating organisms have swimming velocity described in (5) when z_0 equal zero. In this case the swimming velocity is diminishing toward the surface.

[25] d) Vertical migration

[26] Vertical migration of dinoflagellates exhibits variable behavior depending on many environmental factors [*Smayda*, 2010b; *Kudela et al.*, 2010]. In many cases, the timing of vertical migrations coincides with the light regime, and it was observed that dinoflagellates actively avoid light intensities higher than a specific light intensity threshold. For example, the light intensity threshold is reported at 10% of the surface PAR by *Heaney and Furnass* [1980] and at 5% by *Liu et al.* [2001]. The diel migration of the dinoflagellates can be modeled as swimming downward (equation (4)) during dark time (from 02Z to 14Z in the Monterey Bay). During light time (from 00Z to 02Z and from 14Z to 24Z), the diel migration can be modeled as the depth directed swimming (equation (5)), where z_0 equals to the light tolerance threshold depth.

[27] In the present paper we intend to use equations (3)–(5) to address the main question of the paper: whether modeling of bioluminescent dinoflagellates swimming behavior can reproduce the observed dynamics during the August 2003 upwelling event: that bioluminescent dinoflagellates from the northern part of the Bay were able to avoid strong advection by southward flow along the entrance to the Bay.

[28] We want to stress here that the actual dinoflagellates swimming behavior depends on many factors including: physical conditions, light intensity, prey pressure, food availability, etc. [see, e.g., *Smayda*, 2000; *Kamykowski et al.*, 1988]. Simulation of actual dinoflagellates swimming can be achieved by modeling values of w_o, z_0 and z_w as functions of environmental conditions (temperature, light intensity, etc.) in formulations (4)–(5). This is a very challenging task due to high uncertainty in parameterizations of such functions. In the present study, we use values of swimming velocities in (4)–(5), which are in the observed ranges [*Smayda*, 2010b, 2000] for the dinoflagellates species observed during the August 2003 upwelling event.

[29] The main question of the paper can be investigated by integrating (3) with initial conditions $C_0(x_0, y_0, z_0, t_0)$ representing the observed population of dinoflagellates in the SA at the beginning of upwelling. The resulting dinoflagellates concentration $C(x, y, z, t)$ can be estimated in the area around mooring M1, for example, with the following functional J:

$$J = \frac{\int_V C(\tau, t)d\tau}{\int_V d\tau} \tag{6}$$

Table 2. Description of Adjoint Runs[a]

	Swimming	Speed (m/day)	Decay Rate (per day)	Ratio (%)
Run 1	none	0	0	100
Run 2	equation (4)	20	0	36
Run 3	equation (5)	20	0	41
Run 4	diel migration	20	0	46
Run 5	equation (4)	8	0	67
Run 6	equation (5)	8	0	70
Run 7	none	0	−0.1/84000	90

[a]Ratios (in %) of J_A (9) to J_A for the Run 1 (no swimming). Ratios are estimated for 24 h prior to the 15 August 00Z.

where V is a domain, which consists of 3 by 3 horizontal grids (approximately an area of 4 km by 4 km) around the mooring M1 down to a depth of 25 m (the depth to which high chlorophyll and backscatter values and weak BL signal were observed), where τ is the location in the model domain V with coordinates (x, y, z), and $d\tau$ is a volume element. The function J is the normalized content of tracer C in the domain around mooring M1 at time t. If the value of (6) is close to zero (normalized content of tracer around mooring M1 is close to zero), that means that in accord with the model (3) the dinoflagellates are able to avoid strong currents and advection to the area around mooring M1 by a combination of swimming behavior and decay of population.

[30] The main challenge with the forward integration of the model (3) is that there is high level of uncertainty in the initial distribution of dinoflagellates in the northern part of the bay (SA area) at the start of the upwelling event (only limited AUV sampling is available to build the initial distribution). However, this knowledge of the initial distribution of the dinoflagellates in the northern part of the Bay is not needed if we use an adjoint to the model (3). As shown by *Shulman et al.* [2011], the adjoint to the tracer model shows where the model water masses originate before being circulated to the area of interest. By using the adjoint for the tracer equation (3), the gradient of the function J (6) at time t with respect to the initial concentration C_0 at time t_0, can be estimated:

$$s = \frac{\partial J}{\partial C_0} \tag{7}$$

where s is the sensitivity, and $\frac{\partial J}{\partial C_0}$ is the gradient of J (at time t) with respect to initial conditions. Sensitivity, s, is a function of location $\tau_0 = \{x_0, y_0, z_0\}$ and times, t_0 and t. The function $s(\tau_0, t_0, t)$ can be called the adjoint tracer distribution (because the function s, is the result of the adjoint tracer model integration).

[31] If we introduce some finite perturbation ΔC_0 at location $\tau_0 = \{x_0, y_0, z_0\}$ to the initial concentration C_0 at time t_0, according to (7) we would have:

$$\Delta J = s(\tau_0, t_0, t) \cdot \Delta C_0(\tau_0, t_0) \tag{8}$$

[32] According to (6) and (8), the adjoint tracer distribution $s(\tau_0, t_0, t)$ represents a fraction of tracer ΔC_0, which makes its way to the volume V from time t_0 to time t. Due to the linearity of (3) and its adjoint problems, the adjoint tracer distribution $s(\tau_0, t_0, t)$ will represent the fraction of the initial tracer concentration that makes its way from location (x,y,z) at time t_0 to the volume V at time t. Sensitivity $s(\tau_0, t_0, t)$ can be estimated by seeding the adjoint variable with a unit value at each grid point in the volume V at time t, and integrating the adjoint of the tracer model backward in time to time t_0 [*Fukumori et al.*, 2004; *Shulman et al.*, 2011]. We initialize the adjoint to the model (3) with a unit value in volume V at time t equals 15 August 00Z (when high chlorophyll and backscatter values and weak BL were observed by AUV). Then, we integrate the adjoint backward in time to t_0 equals 14 August 00Z (24 h prior to 15 August 00Z), as a result, $s(\tau_0, t_0, t)$ will represent a fraction of the initial tracer concentration (dinoflagellates concentration) circulated from time 14 August 00Z to the volume V at time 15 August 00Z.

[33] The following metric can be used to compare adjoint runs with different swimming behaviors and decay rates in (3):

$$J_A(t_0) = \frac{\int\limits_{SA} s(\tau_0, t_0, t) d\tau_0}{\int\limits_{SA} d\tau_0}, \tag{9}$$

where t is equal to 15 August 00Z, *SA* is, as we defined before, the shadow area in the northern part of the Bay (Figure 1). The SA consists of the model grid cells between 122.1 W and 121.9 W and from 36.91 N to the coast, τ_0 is the location in the *SA* domain with coordinates $\{x_0, y_0, z_0\}$, and $d\tau_0$ is a volume element of *SA*. In accord with our discussions about the adjoint to (3), the metrics J_A is proxy of how much of tracer concentration from the shadow area circulated to the area around mooring M1 (domain V) from time t_0 to time t (15 August 00Z): the smaller value of the J_A indicates the less advection of the tracer from the SA area to the area around mooring M1 (domain V).

[34] Using the adjoint to (3) is more beneficial than the forward problem (3) because initial conditions for the adjoint integration are uniquely determined by seeding unit adjoint into the domain V, while for the forward integration of the model (3), we need accurate representation of initial distribution of the concentration of dinoflagellates in the northern part of the Bay (SA area).

4. Results

[35] During August, 2003, a variety of bioluminescent dinoflagellates species were observed in the Monterey Bay area, among them *Lingulodinium polyedrum*, *Ceratium fusus*, *Protoperidinium*, *Dinophysis* and *Alexandrium*. The observed swimming speeds are: around 278 μm s^{-1} (24 m/day) for *Lingulodinium polyedrum* and *Ceratium fusus* [*Smayda*, 2010b]; from around 8 m/day to 30 m/day for *Protoperidinium* dinoflagellates [*Smayda*, 2000, Figure 9]. *Dinophysis* and *Alexandrium* reported observed swimming speeds reaching 40 m/day.

[36] Table 2 list attributes of the considered here adjoint runs. Runs differ in swimming behaviors, values of swimming speed and decay rate values. For our studies, the swimming behaviors (4) and (5) are used. Two values for swimming velocities w_o in (4) and (5) are considered: 20 m/day, which is in the middle range of swimming velocities for the observed dinoflagellates species, and

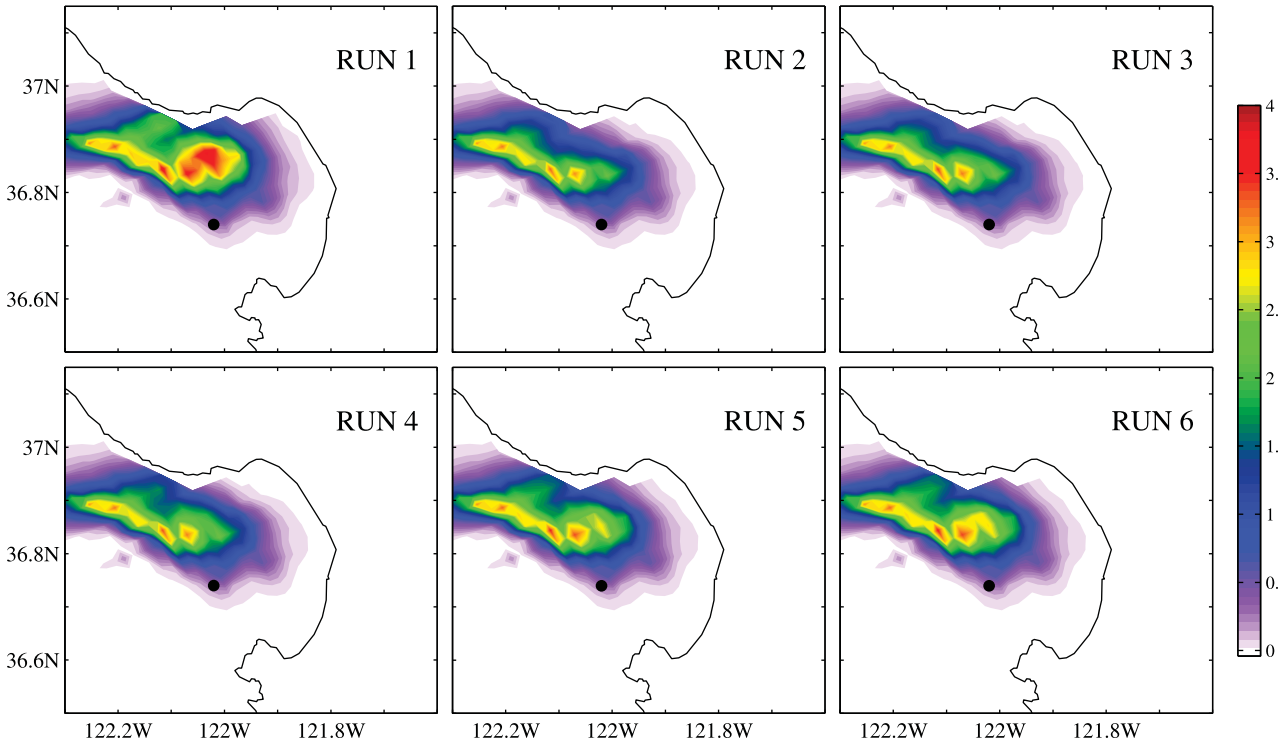

Figure 3. Vertically integrated (up to 25 m depth) adjoint tracer distributions for Runs 1–6 considered in Table 2. Distributions are at 14 August 00Z of 2003 (at 24 h prior to 15 August 00Z, 2003), units are in m.

8 m/day which is at the lowest range of the dinoflagellates swimming velocity. The values of z_0 is chosen as the averaged observed euphotic depth in the Bay. In accord with *Lee et al.* [2007], z_0 is 20 m. The value of z_w is chosen 2.5 m. We found a very low sensitivity of results to the values of z_0 and z_w: 20% change in z_0 leads to an approximately 3.7% change in results, and 20% change in z_w leads to an approximately 0.1% change in results. To simulate diel vertical migration in accord with the section 3.3, the light tolerance threshold depth is chosen as an averaged depth of 10% of the surface PAR [*Heaney and Furnass*, 1980]. With averaged depth of the euphotic depth equals 20 m, the depth of 10% of the surface PAR is around 10 m.

[37] As stated by *Smayda* [2010a], dinoflagellates exhibit strong survival skills. Therefore, it is unlikely that the observed weak BL signal at mooring M1 is a result of mortality during advection (transition) from SA area along the entrance to the Bay to the area around mooring M1 (which takes about 12 h for a particle to be advected from the SA domain to the mooring M1). In all except Run 7, we used decay rate μ equal 0. For run 7, $\mu = -0.1/(84000)$ was used (which represents 10% decay of the population per day).

[38] In accord with the section 3.3, all adjoint runs were initialized on August 15th 00Z with a unit value seeded into the area (V) around mooring M1, which, as stated in section 3.3, consists of 3 by 3 horizontal grids (approximately area of 4 km by 4 km) down to depth 25 m (the depth to which high chlorophyll and backscatter values and weak BL signal were observed on 15 August).

[39] Metric (9) is used to compare adjoint runs listed in Table 2. As stated in section 3.3, the metric J_A is a proxy of how much of tracer concentration from the shadow area (SA) had circulated to the area around mooring M1 (domain V) from time t_0 to time t equals August 15th 00Z.

[40] Run 1 is the adjoint run without swimming (Table 2). Values of J_A for other runs were normalized by the value of J_A for Run 1. Results are shown in Table 2 for times t_0 equal 24 h prior to August 15th 00Z, therefore for August 14 00Z.

[41] For Runs 2, 3 and 4, the values J_A (9) are 36%, 41% and 46% of the J_A value for Run 1. This means that in the case of dinoflagellates swimming at ~20 m/day, only 36% to 46% of the SA population will be advected to the M1 area, in comparison to the case of no swimming. This corresponds with the observed ratio of 45% for observed mean BL values in SA and M1 areas (Table 1). Therefore, the observed ratio of BL signals in SA and M1 areas on August 15th can be explained by the ability of bioluminescent dinoflagellates to swim with the velocity in the range of average swimming velocity for observed species. For Runs 5 and 6 (swimming with the speed 8 m/day, which is minimal observed swimming velocity for the observed dinoflagellates species), the values of J_A (9) are around 70% of the J_A value for Run 1. The value of J_A (8) for Run 7 is 90% of the J_A value for Run 1.

[42] Figure 3 shows vertically integrated adjoint maps for 24 h prior to 15 August 2003 for runs 1–6 considered in Table 2. They show that for Runs 2, 3 and 4 (with the swimming speed in the range of average observed swimming velocity for observed dinoflagellates species), the tracer concentration that circulated into the M1 area mostly

Table 3. Description of Forward Runs[a]

	Swimming	Speed (m/day)	Decay Rate (per day)	Ratio (%)
Run 8	none	0	0	100
Run 9	equation (4)	20	0	51
Run 10	equation (5)	20	0	53
Run 11	diel migration	20	0	57

[a]Ratios (in %) of J (6) to J for the Run 8 (no swimming). Ratios are estimated for 24 h of forward simulations (15 August 00Z).

originated along the entrance to the Bay and to the west, but not from the SA area.

[43] To further verify our results from the adjoint runs, we have conducted forward simulations with (3)–(5). As stated in section 3.3, forward simulations are complicated by the high uncertainty in the initial distribution of the dinoflagellates population in the SA. As stated in section 3.2, the BL model (1) was initialized on 14 August with assimilation of available AUVs bioluminescence surveys data into (1)–(2). We use this initial BL distribution as a proxy of initial dinoflagellates distribution in the shadow area for model (3) on 14 August 00Z. However, as we mentioned previously in section 3.2, this initial BL distribution has a high concentration along the entrance to the Bay. For this reason, the initial distribution is equal to the BL concentration from the BL model (section 3.2) in the SA only, and equals zero elsewhere. In this case, with forward simulations (3)–(5), we can verify how much tracer concentration from the shadow area is advected to the area along the entrance to the Bay and to the area around mooring M1. The list of four forward runs' attributes is presented in Table 3. For evaluation and comparison of forward runs, we used function J (6) from section 3.3.

[44] As we recall, the observed ratio of the mean BL signal in the shadow area to the mean BL around mooring M1 was 45%, while the BL model (without swimming) showed the ratio 89%. In accord with Table 3, values of J (6) for all runs with swimming (speed 20 m/day) are about 50–57% of the value of J for the run 8 without swimming. This makes the ratio for runs with swimming around $89\% \times 50\% = 45\%$, which agrees with the observations. This supports our derivations and conclusions from adjoint runs. Figure 4 shows vertically integrated (up to 25 m depth) concentration maps for 24 h of forward simulations (15 August 2003) for the runs considered in Table 3. They demonstrate less than half of the advection of concentration from the SA area to the M1 area for runs with swimming in comparison to the Run 8 without swimming.

5. Conclusions

[45] During the development of upwelling in the Monterey Bay area, the observed offshore water masses (in the area around mooring M1 at the entrance to the Bay) with the subsurface layer of bioluminescent zooplankton were replaced by water masses with a relatively high presence of mostly non-bioluminescent phytoplankton, which was advected from the northern coast of the Bay. The bioluminescent dinoflagellates from the northern part of the Bay were able to avoid advection by southward flowing currents along the entrance to the Monterey Bay into the M1 area, while non-bioluminescent phytoplankton was advected. It is

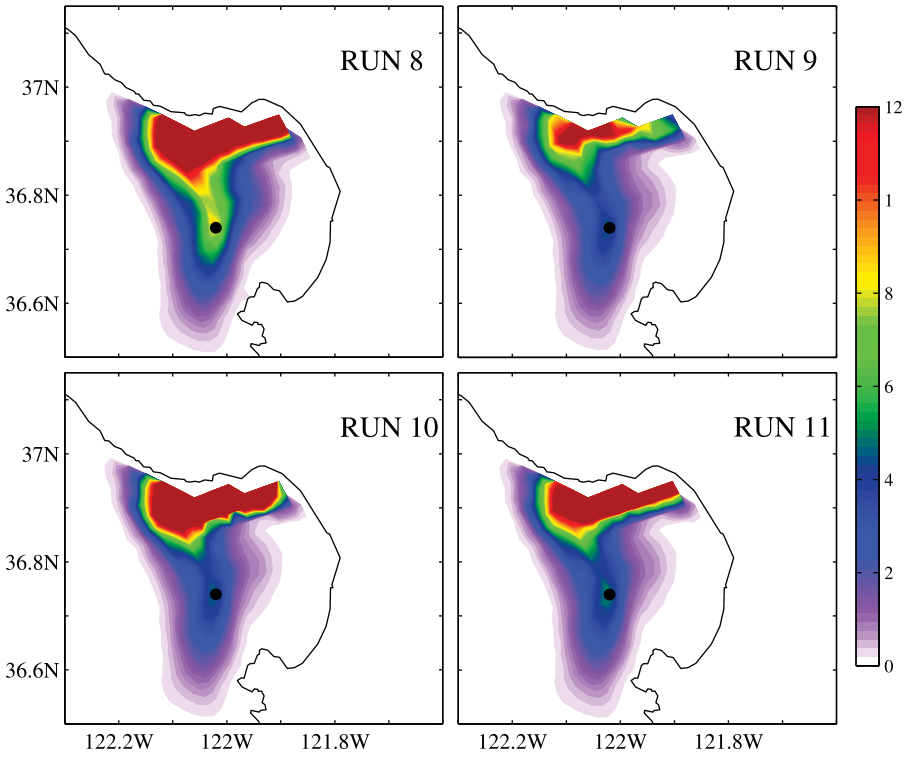

Figure 4. Vertically integrated (up to 25 m depth) concentrations maps for Runs 8–11 considered in Table 3. Integrated concentrations are at 15 August 00Z, 2003 (at 24 h of forward simulations). Values are normalized by 10^9, units are photons m/s.

known [e.g., see *Smayda*, 2010b] that vertical swimming of dinoflagellates to deeper layers helps them avoid losses due to advection. In the present paper, we tested the hypothesis that vertical swimming behavior explains observed ability of dinoflagellates' to avoid advection by strong currents. The dynamics of dinoflagellates is modeled with the tracer model where the dinoflagellate population is modeled as a concentration, and vertical swimming velocity is introduced into the tracer advective-diffusive-reaction model. Three swimming behaviors are considered here: sinking, swimming to the target depth and diel vertical migration. Swimming velocities in all cases are considered in the range of documented velocities for the dinoflagellates species observed during the upwelling development in the Monterey Bay. It is shown that with swimming at a speed 20 m/day (which is in the middle of the swimming velocities ranges for observed dinoflagellates species), approximately 40% of tracer concentration from the northern part of the Bay will be advected in comparison to the case without swimming. This is in agreement with the observed ratio of mean BL intensity in the northern part of the Bay to the BL intensity at the M1 location (Table 1) which is 45%. Therefore, dinoflagellates swimming with the speed around the middle of the observed range of swimming velocities could avoid advection to the area around mooring M1 during the upwelling development. The mechanism for dinoflagellate retention in northern Monterey Bay presented here is also consistent with the observed seasonal persistence of dinoflagellates [*Ryan et al.*, 2005, 2009].

[46] Therefore, our modeling studies have demonstrated that the observed dinoflagellates' avoidance of advection by the southward flowing jet along the entrance to the Bay can be explained by the dinoflagellates' ability to swim vertically. This complicates even short-term (1 day) modeling and predictions of underwater light, BL and water leaving radiances. Examples presented here and by *Shulman et al.* [2011] demonstrate that advective processes alone might identify plankton aggregations, but do not accurately predict even shot-term changes (1 day) in horizontal and vertical redistributions of these populations, especially in cases when plankton swimming behavior is involved.

[47] One of our future research topics will be the modeling of dinoflagellates' actual swimming behavior. In the present paper, we have used swimming velocities which are in the observed ranges of swimming velocities for dinoflagellates population during the upwelling. The actual dinoflagellates' swimming behavior depends on many factors such as physical conditions, light, prey pressure, food availability, etc. [see, e.g., *Smayda*, 2000], and require derivations of functional relations between environmental conditions and plankton swimming behavior.

[48] We want to note that the model simulations did not include tides, which may play a role in biological advection, particularly around the canyon, and their inclusion will be another topic in our future research. The parameterization of vertical mixing might be important for modeling dinoflagellates distributions. As stated in section 3.1, the Mellor-Yamada level 2.5 turbulence closure scheme is used in the present study. One of the topics of future research will also be the study of the impact of different mixing parameterization schemes on dinoflagellates' dynamics.

[49] **Acknowledgments.** This research was funded through the Naval Research Laboratory (NRL) projects, "Bio-optical studies of predictability and assimilation in the coastal environment (BIOSPACE)" and "Modeling Dynamic Bio-Optical Layers In Coastal Systems (DYaBOLIC)" under program element 61153N and grants N0001411WX20051, N0001410WX20482, N0001409AF00002, and N0001410AF00002 sponsored by the Office of Naval Research, Marine Mammals and Biology Program. We thank the anonymous reviewers, who provided very insightful comments and recommendations to improve the paper. Computer time for the numerical simulations was provided through a grant from the Department of Defense High Performance Computing Initiative. This manuscript is NRL contribution 7330-11-785.

References

Barron, C. N., A. B. Kara, H. E. Hurlburt, C. Rowley, and L. F. Smedstad (2004), Sea surface height predictions from the Global Navy Coastal Ocean Model (NCOM) during 1998–2001, *J. Atmos. Oceanic Technol.*, *21*, 1876–1893, doi:10.1175/JTECH-1680.1.

Chai, F., R. C. Dugdale, T.-H. Peng, F. P. Wilkerson, and R. T. Barber (2002), One-dimensional ecosystem model of the equatorial Pacific upwelling system. Part I: model development and silicon and nitrogen cycle, *Deep Sea Res., Part II*, *49*, 2713–2745, doi:10.1016/S0967-0645(02)00055-3.

Cummings, J. A. (2005), Operational multivariate ocean data assimilation, *Q. J. R. Meteorol. Soc.*, *131*, 3583–3604, doi:10.1256/qj.05.105.

Doyle, J. D., Q. Jiang, Y. Chao, and J. Farrara (2009), High-resolution real-time modeling of the marine atmospheric boundary layer in support of the AOSN-II field campaign, *Deep Sea Res., Part II*, *56*(3–5), 87–99.

Fox, D. N., C. N. Barron, M. R. Carnes, M. Booda, G. Peggion, and J. Van Gurley (2002), The Modular Ocean Data Assimilation System, *Oceanography*, *15*(1), 22–28.

Franks, P. J. S. (1992), Sink or swim: Accumulation of biomass at fronts, *Mar. Ecol. Prog. Ser.*, *82*, 1–12, doi:10.3354/meps082001.

Fukumori, I., T. Lee, B. Cheng, and D. Menemenlis (2004), The origin, pathway, and destination of Niño-3 water estimated by a simulated passive tracer and its adjoint, *J. Phys. Oceanogr.*, *34*, 582–604, doi:10.1175/2515.1.

Graham, W. M., and J. L. Largier (1997), Upwelling shadows as nearshore retention sites: The example of northern Monterey Bay, *Cont. Shelf Res.*, *17*, 509–532, doi:10.1016/S0278-4343(96)00045-3.

Heaney, S. I., and T. I. Furnass (1980), Laboratory models of diel vertical migration in the dinoflagellate *Ceratium hirundinella*, *Freshwater Biol.*, *10*, 163–170, doi:10.1111/j.1365-2427.1980.tb01190.x.

Hines, A., and P. D. Killworth (2001), A inversion-assimilation approach using hydrographic data in coarse-resolution ocean model, *J. Atmos. Oceanic Technol.*, *18*, 1503–1520, doi:10.1175/1520-0426(2001)018<1503:AIAAUH>2.0.CO;2.

Kamykowski, D., S. A. McCollum, and G. J. Kirkpatrick (1988), Observations and a model concerning the translational velocity of a photosynthetic marine dinoflagellates under variable environmental conditions, *Limnol. Oceanogr.*, *33*(l), 66–78.

Kudela, R. M., S. Seeyave, and W. P. Cochlan (2010), The role of nutrients in regulation and promotion of harmful algal blooms in upwelling systems, *Prog. Oceanogr.*, *85*, 122–135, doi:10.1016/j.pocean.2010.02.008.

Lee, Z. P., A. Weidemann, J. Kindle, R. Arnone, K. L. Carder, and C. Davis (2007), Euphotic zone depth: its derivation and implication to ocean-color remote sensing, *J. Geophys. Res.*, *112*, C03009, doi:10.1029/2006JC003802.

Liu, G., G. S. Janowitz, and D. Kamykowski (2001), A biophysical model of population dynamics of the autotrophic dinoflagellate *Gymnodinium breve*, *Mar. Ecol. Prog. Ser.*, *210*, 101–124, doi:10.3354/meps210101.

Martin, P. J. (2000), Description of the Navy Coastal Ocean Model Version 1.0, *NRL/FR/732-00-9962*, Naval Res. Lab., Stennis Space Cent., Mississippi.

Moline, M. A., S. M. Blackwell, J. F. Case, S. H. D. Haddock, C. M. Herren, C. M. Orrico, and E. Terrill (2009), Bioluminescence to reveal structure and interaction of coastal planktonic communities, *Deep Sea Res., Part II*, *56*(3–5), 232–245, doi:10.1016/j.dsr2.2008.08.002.

Penta, B., Z. Lee, R. Kudela, S. Palacios, D. Gray, J. Jolliff, and I. Shulman (2008), An underwater light attenuation scheme for marine ecosystem models, *Opt. Express*, *16*, 16,581–16,591.

Ramp, S. R., et al. (2009), Preparing to predict: The second Autonomous Ocean Sampling Network (AOSN-II) experiment in the Monterey Bay, *Deep Sea Res., Part II*, *56*, 68–86, doi:10.1016/j.dsr2.2008.08.013.

Rhodes, R. C., et al. (2002), Navy real-time global modeling systems, *Oceanography*, *15*(1), 29–43.

Rosmond, T. E., J. Teixeira, M. Peng, T. F. Hogan, and R. Pauley (2002), Navy Operational Global Atmospheric Prediction System (NOGAPS): Forcing for ocean models, *Oceanography*, *15*, 99–108.

Ryan, J. P., H. M. Dierssen, R. M. Kudela, C. A. Scholin, K. S. Johnson, J. M. Sullivan, A. M. Fischer, E. V. Rienecker, P. R. McEnaney, and F. P. Chavez (2005), Coastal ocean physics and red tides: An example from Monterey Bay, California, *Oceanography*, *18*, 246–255.

Ryan, J. P., J. F. R. Gower, S. A. King, W. P. Bissett, A. M. Fischer, R. M. Kudela, Z. Kolber, F. Mazzillo, E. V. Rienecker, and F. P. Chavez (2008), A coastal ocean extreme bloom incubator, *Geophys. Res. Lett.*, *35*, L12602, doi:10.1029/2008GL034081.

Ryan, J. P., A. M. Fischer, R. M. Kudela, J. F. R. Gower, S. A. King, R. Marin III, and F. P. Chavez (2009), Influences of upwelling and downwelling winds on red tide bloom dynamics in Monterey Bay, California, *Cont. Shelf Res.*, *29*, 785–795, doi:10.1016/j.csr.2008.11.006.

Shulman, I., D. J. McGillicuddy Jr., M. A. Moline, S. H. D. Haddock, J. C. Kindle, D. Nechaev, and M. W. Phelps (2005), Bioluminescence intensity modeling and sampling strategy optimization, *J. Atmos. Oceanic Technol.*, *22*, 1267–1281.

Shulman, I., J. Kindle, P. Martin, S. deRada, J. Doyle, B. Penta, S. Anderson, F. Chavez, J. Paduan, and S. Ramp (2007), Modeling of upwelling/relaxation events in the coastal ocean, *J. Geophys. Res.*, *112*, C06023, doi:10.1029/2006JC003946.

Shulman, I., et al. (2009), Impact of glider data assimilation on the Monterey Bay model, *Deep Sea Res., Part II*, *56*(3–5), 128–138.

Shulman, I., S. Anderson, C. Rowley, S. deRada, J. Doyle, and S. Ramp (2010), Comparisons of upwelling and relaxation events in the Monterey Bay area, *J. Geophys. Res.*, *115*, C06016, doi:10.1029/2009JC005483.

Shulman, I., M. A. Moline, B. Penta, S. Anderson, M. Oliver, and S. H. D. Haddock (2011), Observed and modeled bio-optical, bioluminescent, and physical properties during a coastal upwelling event in Monterey Bay, California, *J. Geophys. Res.*, *116*, C01018, doi:10.1029/2010JC006525.

Smayda, T. J. (2000), Ecological features of harmful algal blooms in coastal upwelling ecosystems, *S. Afr. J. Mar. Sci.*, *22*, 219–253, doi:10.2989/025776100784125816.

Smayda, T. J. (2010a), Adaptations and selection of harmful and other dinoflagellates species, in upwelling systems. 1. Morphology and adaptive polymorphism, *Prog. Oceanogr.*, *85*, 53–70, doi:10.1016/j.pocean.2010.02.004.

Smayda, T. J. (2010b), Adaptations and selection of harmful and other dinoflagellates species, in upwelling systems. 2. Motility and migratory behavior, *Prog. Oceanogr.*, *85*, 71–91, doi:10.1016/j.pocean.2010.02.005.

Stock, S. A., D. J. McGillicuddy, A. R. Solow, and D. M. Anderson (2005), Evaluating hypotheses for the initiation and development of Alexandrium fundyense blooms in the western Gulf of Maine using a coupled physical–biological model, *Deep Sea Res., Part II*, *52*, 2715–2744, doi:10.1016/j.dsr2.2005.06.022.

S. Anderson, B. Penta, P. Sakalaukus, and I. Shulman, Oceanography Division, Naval Research Laboratory, Bldg. 1009, Stennis Space Center, MS 39529, USA. (igor.shulman@nrlssc.navy.mil)

S. H. D. Haddock, Monterey Bay Aquarium Research Institute, 7700 Sandholdt Rd., Moss Landing, CA 95039, USA.

M. A. Moline, Center for Marine and Coastal Sciences, Biological Sciences Department, California Polytechnic State University, San Luis Obispo, CA 93407, USA.

M. J. Oliver, College of Earth, Ocean and Environment, University of Delaware, 700 Pilottown Rd., Lewes, DE 19958, USA.